SECURITY INFORMATION

[redacted]

221
Copy
RM L52E05a

NACA RM L52E05a

[redacted]

TECH LIBRARY KAFB, NM
0144463

NACA

RESEARCH MEMORANDUM

7332

FLOW SEPARATION FROM RODS AHEAD OF BLUNT NOSES AT MACH NUMBER 2.72

By Jim J. Jones

Langley Aeronautical Laboratory
Langley Field, Va.

Classification cancelled (or changed to UNCLASSIFIED)

By Authority of NASA Tech Pub Announcement #113
(OFFICER AUTHORIZED TO CHANGE)

By ..... 2 Apr 57
GRADE OF OFFICER MAKING CHANGE)

3 Apr 61
DATE

[redacted]

NATIONAL ADVISORY COMMITTEE FOR AERONAUTICS

WASHINGTON

July 15, 1952

[redacted]

TECH LIBRARY KAFB, NM
0144463

NATIONAL ADVISORY COMMITTEE FOR AERONAUTICS

RESEARCH MEMORANDUM

FLOW SEPARATION FROM RODS AHEAD OF BLUNT NOSES AT MACH NUMBER 2.72

By Jim J. Jones

SUMMARY

An experimental investigation in the Langley gas dynamics laboratory has been made of the flow separation from slender rods mounted to extend forward along the axes of symmetry of blunt-nosed bodies. The mechanism of the separation and its governing criteria are discussed. Drag data at a Mach number of 2.72 for various rod lengths and nose radii at an angle of attack of 0° are presented.

It was found that the drag coefficients of blunt noses could be appreciably reduced by the use of protruding rods. Criteria for rod length which gives lowest drag are given.

INTRODUCTION

The desirability of a blunt, rounded nose on a supersonic missile which contains a seeker device is well-known, and a number of investigations have been made of the resultant drag increase. (See, for instance, refs. 1 to 3.) A study of noses in which the tip of a basic ogive is replaced by a near-hemisphere indicates that if the nose radius is less than one-quarter of the maximum radius of the body, the drag increase is not severe. With increasing nose radius, however, the drag increases very rapidly.

The flow in front of a blunt nose has been found to be easily separated from the surface of a slender rod or needle which projects forward of the nose. (See ref. 4.) This separation is a result of the interaction of the bow wave and the boundary layer on the rod. The separated region is found to form approximately a conical shape, and the accompanying shock is very nearly the conical shock expected for a solid cone geometrically similar to the separation region.

If some forward-projecting device can be found which operates satisfactorily under varying conditions of Mach number and angle of attack, practical use of this phenomenon might be made to reduce the drag of blunt-nosed missiles. The purpose of this investigation was to study the separation phenomenon at an angle of attack of 0° so that the factors determining optimum rod length might be understood.

SYMBOLS

C_d	nose-drag coefficient based on maximum frontal area
Δp	pressure rise across shock wave
l	distance from tip of rod to nose of model
q	local dynamic pressure
r_b	radius of model at base
r_n	radius of hemispherical nose
R_x	Reynolds number based on distance x
S	station along model axis measured from tip, in.
S_b	length of basic model, in.
x	distance from tip of rod to point of separation
y	radius at any point on model, in.

MODELS AND TESTS

A sketch of the configurations tested is shown in figure 1. The models were fitted to a small strain-gage drag balance.

Model 1, the basic configuration, represents a nose design which has a minimum wave-drag coefficient for a given fineness ratio according to the slender-body theory. (See ref. 5.) The fineness ratio used for model 1 was 4.0. The ordinates for this type of body follow the equation

$$y^2 = \frac{r_b^2}{\pi}\left[t\sqrt{1 - t^2} + \cos^{-1}(-t)\right] \tag{1}$$

where

$$t = 2\frac{S}{S_b} - 1$$

For model 1 the value of S_b was 4.0 inches and r_b was 0.5 inch.

Models 2, 3, and 4 were designed by replacing the nose point of model 1 with spherical segments having a radius one-quarter, one-half, and three-quarters, respectively, of the base radius. On each model the spherical segment and the unmodified portion of the model were tangent at the meeting point, behind which each model was identical to model 1.

Model 5, a cone cylinder of approximately the same volume and length as model 1, was used merely for comparison of drag with the other configurations.

On models 2 and 3 a small diameter rod of variable length was tested. The diameter of the rod used on model 2 was 0.020 inch and for model 3 the rod diameter was 0.040 inch, so that the ratio of rod diameter to nose radius would be constant. The tip of each rod was a 10° half-angle cone. Figure 2 is a schematic drawing of a model nose with a rod mounted.

All tests were run in a blowdown jet of the Langley gas dynamics laboratory at a Mach number of 2.72. The test section measures 3 by 5 inches. The Reynolds number of the undisturbed flow was 1.83×10^6 per inch and all tests presented were run at an angle of attack of 0°.

The strain-gage balance was read from a Brown potentiometer. Flow was not permitted to enter the sting mount at the rear of the model, and the pressure on the base of the model was measured on a mercury manometer. The coefficients were based on zero base drag.

RESULTS AND DISCUSSION

The drag coefficients of models 1 to 5 were measured on the drag balance. (See fig. 3.) As was previously mentioned, the drag increase is not severe for a value of $\frac{r_n}{r_b} = 0.25$. It is interesting to note that the drag of model 2 $\left(\frac{r_n}{r_b} = 0.25\right)$ is about the same as that of model 5, the cone cylinder.

Figure 4 is a series of shadow photographs showing model 3 with a rod of increasing length. The light parabolic-shaped trace is the intersection of the shock wave and the window. The lines in some of the photographs are caused by a small amount of compressor oil on the surface of the windows. The photographs show that the point of separation remains fairly near the tip of the rod for values of l/r_n up to 3.5. With an additional increase in rod length the separation point jumps to a point downstream on the rod. The distance $l - x$ from the point of separation to the nose of the model has not changed much for values of l/r_n from 3.8 to 6.0. Observe that the base of the separation region almost covers the nose of the model in the photographs.

An explanation of this phenomenon has not been offered yet; however, recent work by Donaldson and Lange (ref. 6) on flow separation gives some insight into the occurrence of this phenomenon. This work relates the Reynolds number and condition of the boundary layer on a flat plate to the minimum pressure rise associated with a shock wave which will cause the boundary layer to separate. In reference 6 it is found that the value of $\Delta p/q$ which will cause the boundary layer to separate is proportional to the skin-friction coefficient. Thus, for the case of the turbulent boundary layer on a flat plate with a one-seventh-power velocity profile

$$(\Delta p/q)_{crit} = A\left(R_x\right)^{-1/5} \tag{2}$$

and for a laminar boundary layer

$$(\Delta p/q)_{crit} = B\left(R_x\right)^{-1/2} \tag{3}$$

where $(\Delta p/q)_{crit}$ is the minimum pressure rise which will cause the boundary layer to separate and A and B are constants with values of 4.44 and 24.6, respectively. The curves of equations (2) and (3) are shown in figure 5. For a boundary layer on a slender shaft, as in the present instance, where the radius of the shaft is not large as compared to the boundary-layer thickness, the preceding work is not directly applicable. However, the results show certain trends which may be used in the present study. Emphasis is placed, first, on the small change in the value of $(\Delta p/q)_{crit}$ with Reynolds number for a turbulent boundary layer as compared with that of a laminar boundary layer and, second, on the appreciable difference in the value of $(\Delta p/q)_{crit}$ for the two curves at any given Reynolds number for the range shown.

If these results are applied to the separation of the boundary layer from the small rod, the conical shock wave which just precedes the point of separation must have exactly that pressure rise which will cause the boundary layer to separate at that particular Reynolds number and type of boundary layer. Consequently, for given conditions and configurations, the separation point may be thought of as determined in the following manner: The cone vertex of the separated region moves forward on the rod (cone angle and Reynolds number R_x decreasing) to that point where a further decrease in cone angle would make the pressure rise insufficient to separate the boundary layer.

For short rod lengths the separation point is determined by the laminar variation of $(\Delta p/q)_{crit}$ with R_x. With increasing rod length the laminar separation point will move back from the rod tip (fig. 6) until the value of R_x for transition is reached. For longer rod lengths, the separation must follow the turbulent variation of $(\Delta p/q)_{crit}$. Since experimental results show that a turbulent boundary layer requires a larger pressure rise in order to separate, the cone angle of the separation must be greater; so, the point of separation "jumps" back on the rod.

In cases where the separation is laminar, the Reynolds number R_x is low. Because of the high Reynolds number per inch at which this experimental work was run, the distance x from the tip of the rod to the point of separation was extremely short. The shadow photographs (fig. 6) of the region were considerably enlarged and show that there is a definite increase in the value of x with increasing rod length. The small arrows indicate the approximate point of separation.

In reference 4 a shock wave was noted to originate near the point where the flow reattaches to the nose. (See fig. 4.) The existence of this shock wave indicates that the border of the separation zone does not meet the nose tangentially and, therefore, must undergo a certain

amount of turning. The flow field in the region of the base of this shock wave follows a pattern similar to that shown

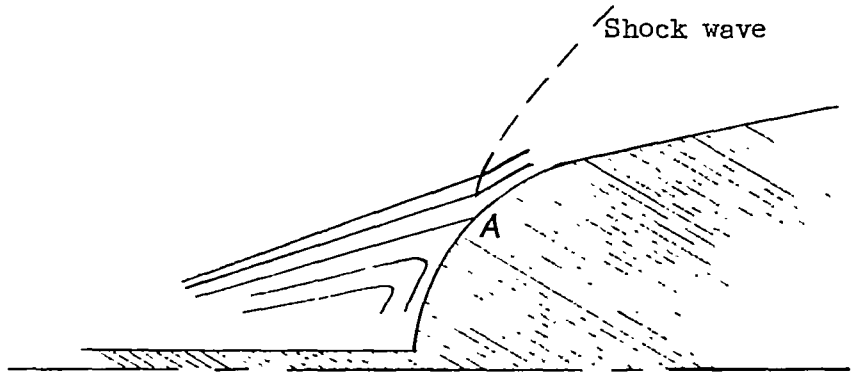

One stream line should exist which intersects the nose at A. This indicates a stagnation point, provided at this point the effect of the local shearing stresses on the flow near the surface balances the effect of the pressure rise across the shock wave. The pressure recovered at A will not be large, but the pressures measured on the surface of the nose (ref. 4) clearly indicate that a maximum is obtained in this region.

Figures 7 and 8 show the decrease in the sum of wave and friction drag obtained on models 2 and 3, respectively, when rods of varying length are mounted. A conclusion may be reached from these figures that the lowest drag is given by the longest rod length for which laminar separation occurred.

CONCLUDING REMARKS

An experimental investigation was made of flow separation from a pointed rod projecting ahead of a blunt nose. It was found that the work of Donaldson and Lange which relates the separation of a boundary layer to the pressure rise across the accompanying shock wave could be used to explain the present phenomenon.

Strain-gage drag tests at a Mach number of 2.72 and at an angle of attack of 0° indicated that the drag of bodies of revolution having near-hemispherical noses could be appreciably reduced through the use of these projecting rods. The lowest drag coefficient obtained with the use of the rods occurred when the boundary layer separated while

still laminar. Thus, the longest rod extension which still maintained laminar separation resulted in the lowest drag coefficient.

Results of drag tests of several noses without projecting rods agreed qualitatively with previous work; that is, the drag increase was very high for large values of the ratio of nose radius to body radius, but for a value of 0.25, the drag increase was small.

Langley Aeronautical Laboratory
National Advisory Committee for Aeronautics
Langley Field, Va.

REFERENCES

1. Hart, Roger G.: Flight Investigation of the Drag of Round-Nosed Bodies of Revolution at Mach Numbers From 0.6 to 1.5 Using Rocket-Propelled Test Vehicles. NACA RM L51E25, 1951.

2. Walchner, O.: Systematic Wind-Tunnel Measurements on Missiles. NACA TM 1122, 1947.

3. Eggers, A. J., Jr., Dennis, David H., and Resnikoff, Meyer M.: Bodies of Revolution for Minimum Drag at High Supersonic Airspeeds. NACA RM A51K27, 1952.

4. Moeckel, Wolfgang E.: Flow Separation Ahead of a Blunt Axially Symmetric Body at Mach Numbers 1.76 to 2.10. NACA RM E51I25, 1951.

5. Von Kármán, Th.: The Problem of Resistance in Compressible Fluids. GALCIT Pub. No. 75, 1936. (From R. Accad. d'Italia, Cl. Sci. Fis., Mat. e Nat., vol. XIV, 1936.)

6. Donaldson, Coleman duP., and Lange, Roy H.: Study of the Pressure Rise Across Shock Waves Required to Separate Laminar and Turbulent Boundary Layers. NACA RM L52C21, 1952.

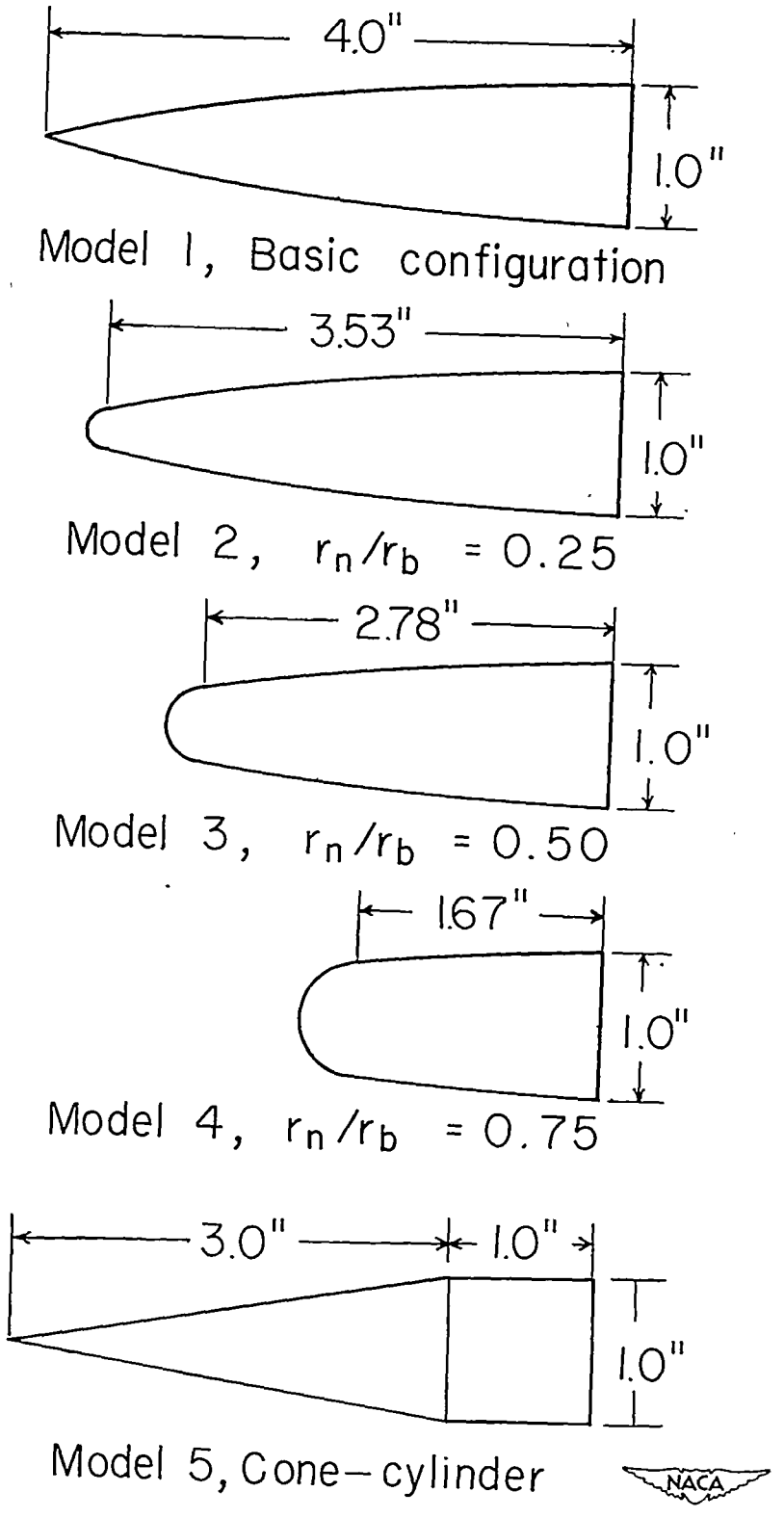

Figure 1.- Sketch of models tested.

[redacted]

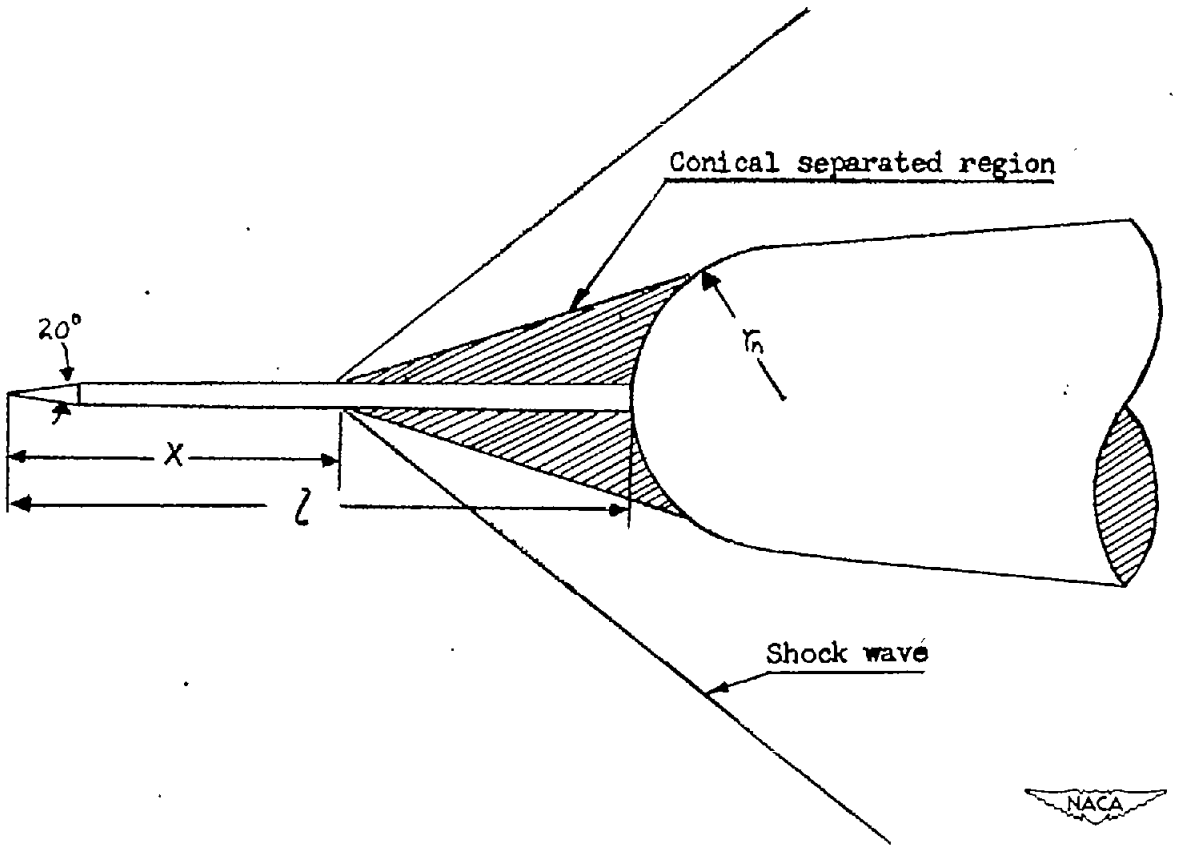

Figure 2.- Schematic drawing of model nose with rod mounted.

[redacted]

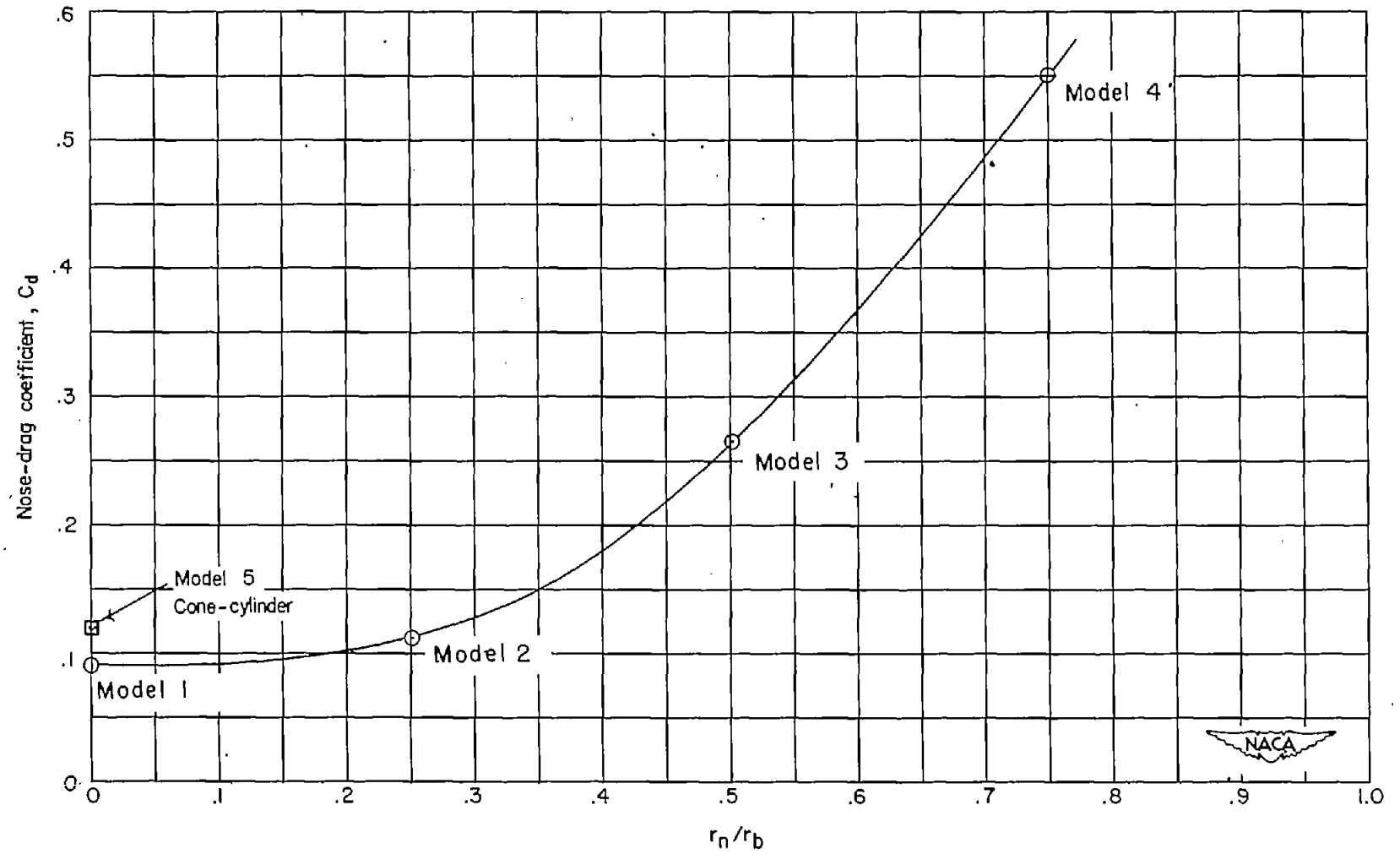

Figure 3.- Effect of nose radius on drag coefficient.

$\frac{l}{r_n} = 1.0$

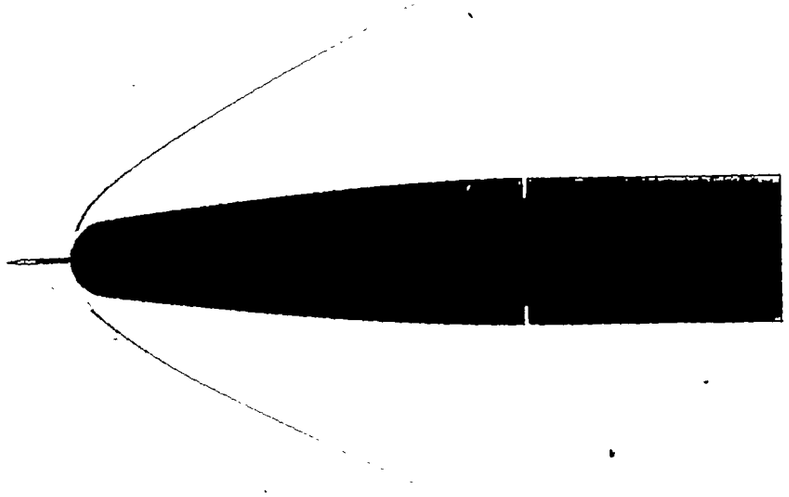

$\frac{l}{r_n} = 1.8$

NACA

L-75098

Figure 4.- Shadow pictures of model 3 showing effects of increasing rod length.

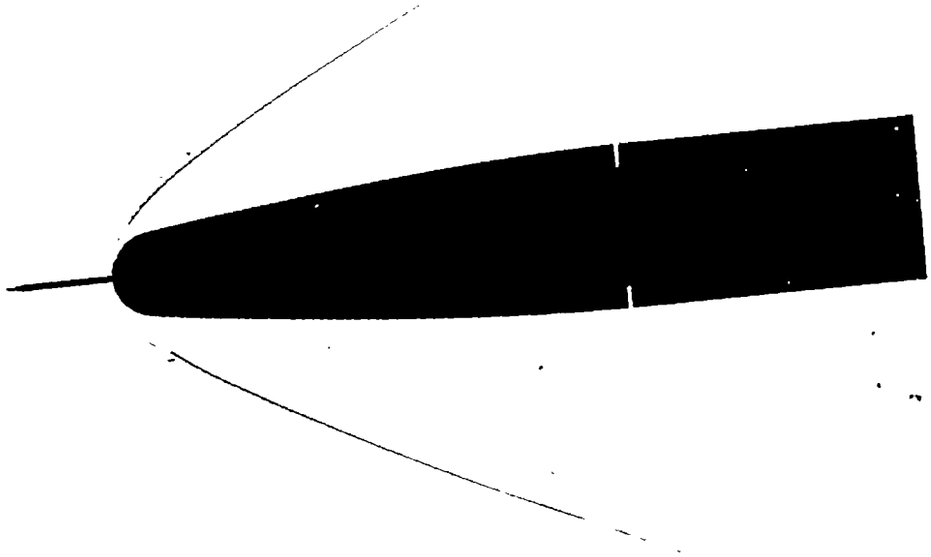

$\frac{l}{r_n} = 2.6$

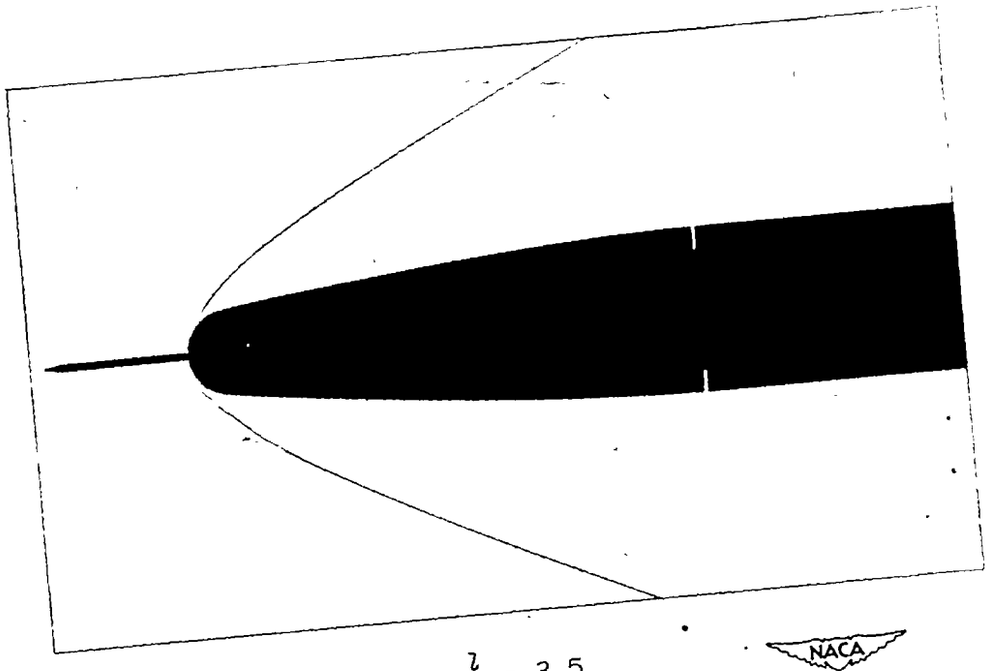

$\frac{l}{r_n} = 3.5$

L-75099

Figure 4.- Continued.

[redacted]

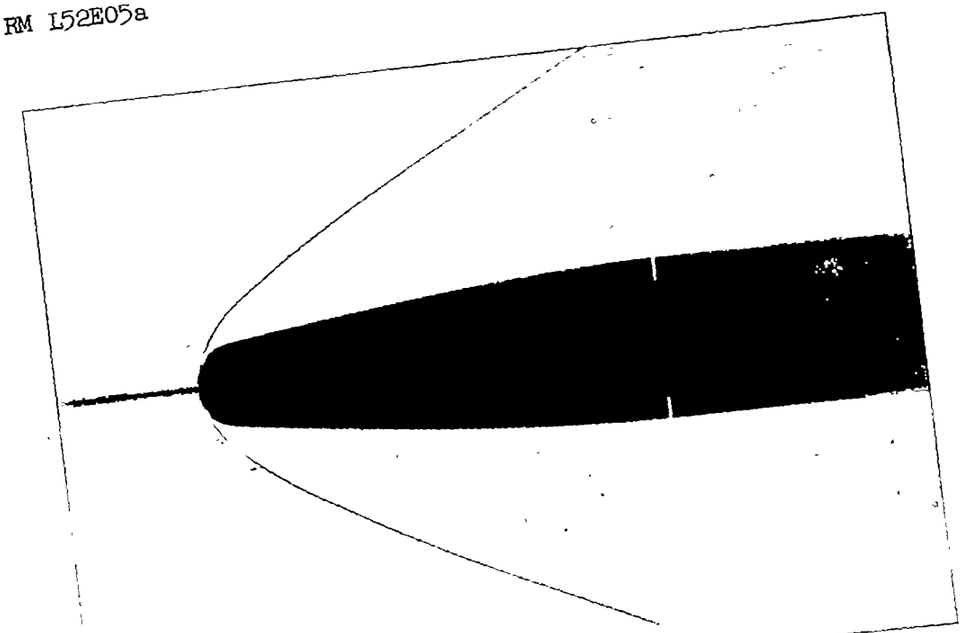

$\frac{l}{r_n} = 3.8$

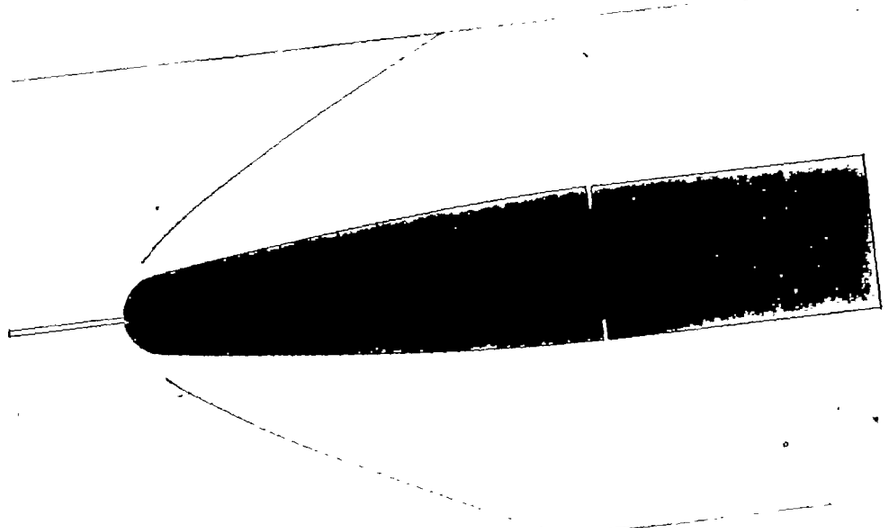

$\frac{l}{r_n} = 6.0$

L-75100

Figure 4.- Concluded.

[redacted]

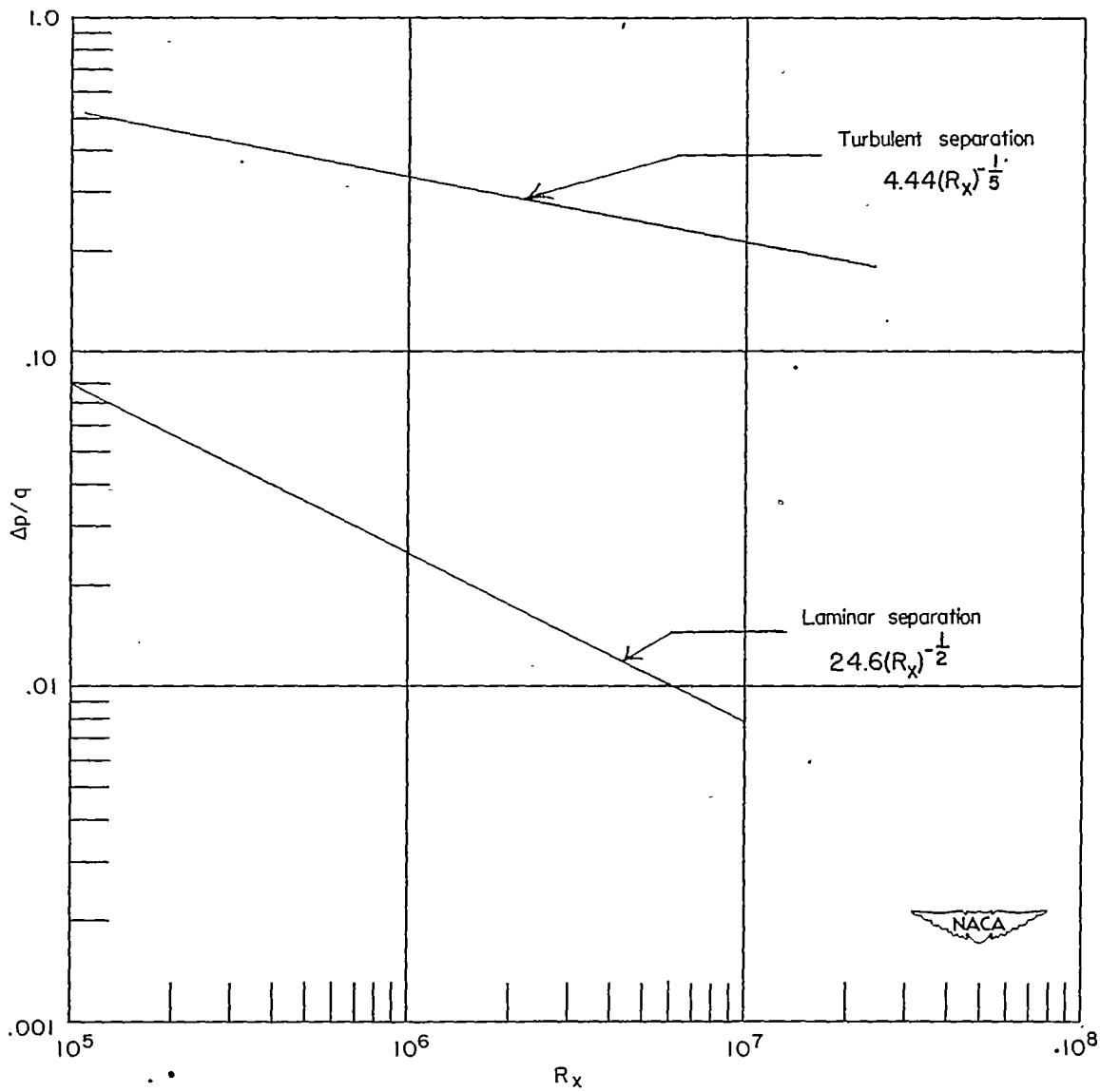

Figure 5.- Empirical flat-plate values of $(\Delta p/q)_{crit}$ against Reynolds number R_x. (From ref. 6.)

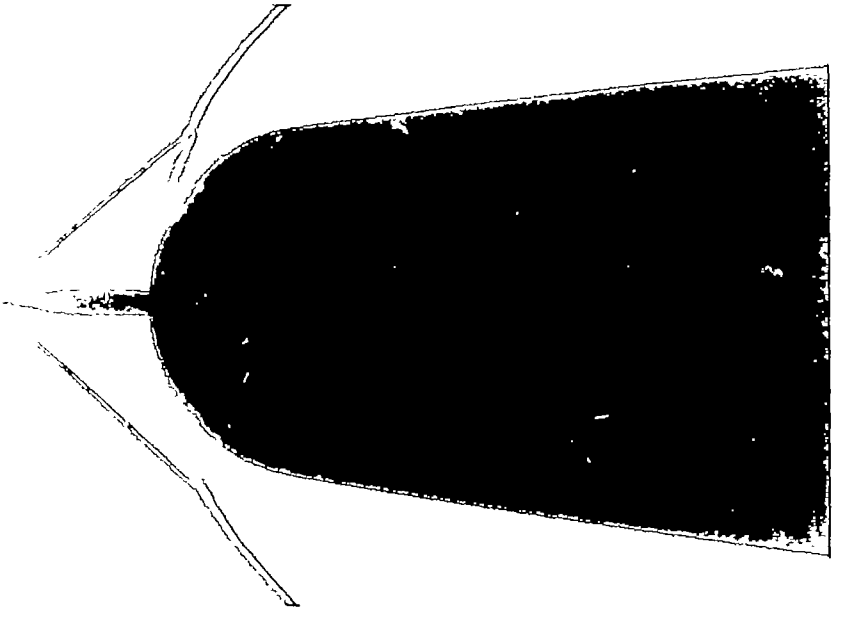

$\frac{l}{r_n} = 1.0$

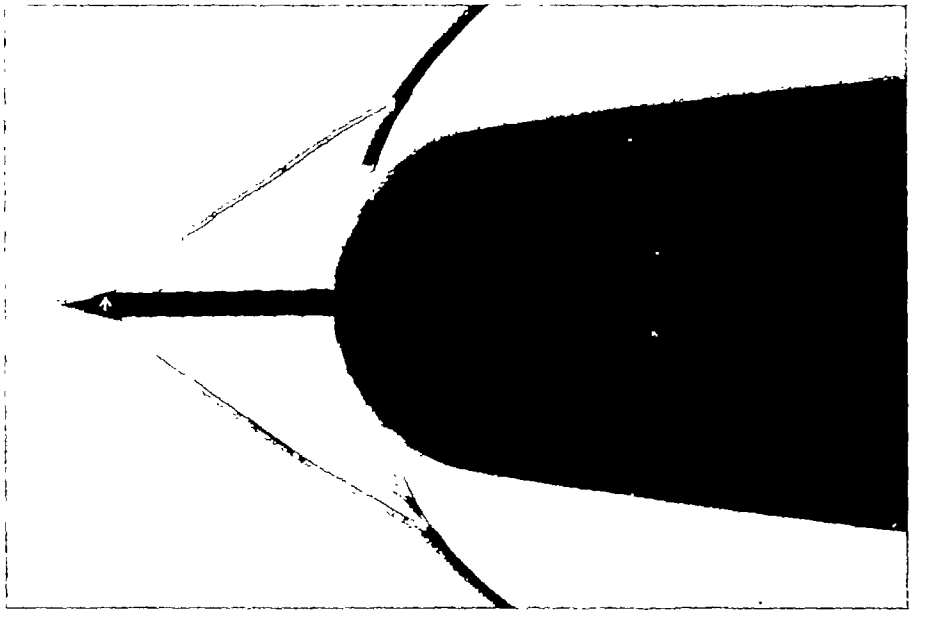

$\frac{l}{r_n} = 1.8$

L-75101

Figure 6.- Enlarged shadow pictures of model 3 showing flow separation from rod. Arrows indicate separation.

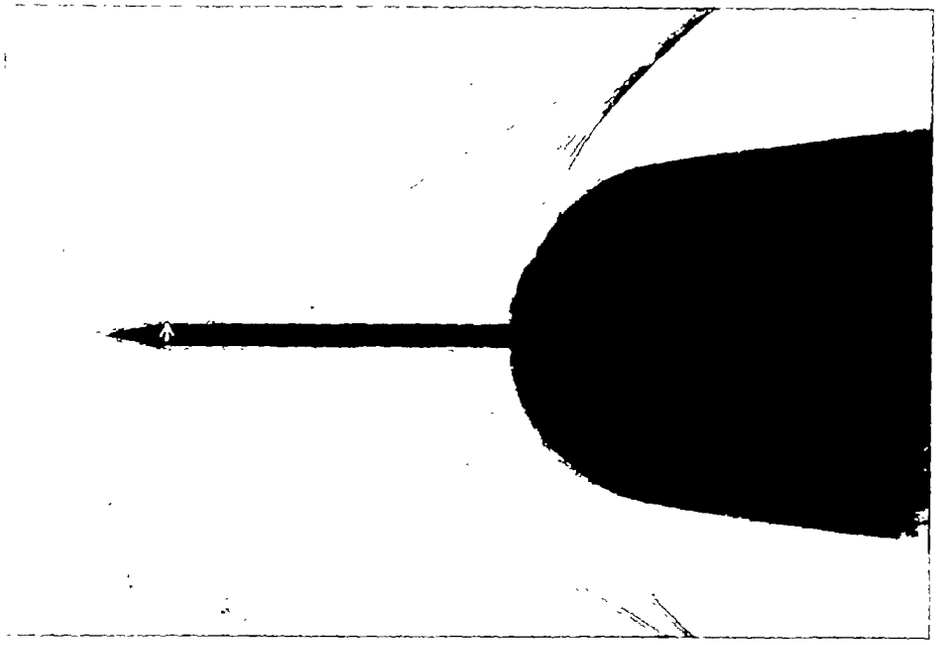

$\frac{l}{r_n} = 2.6$

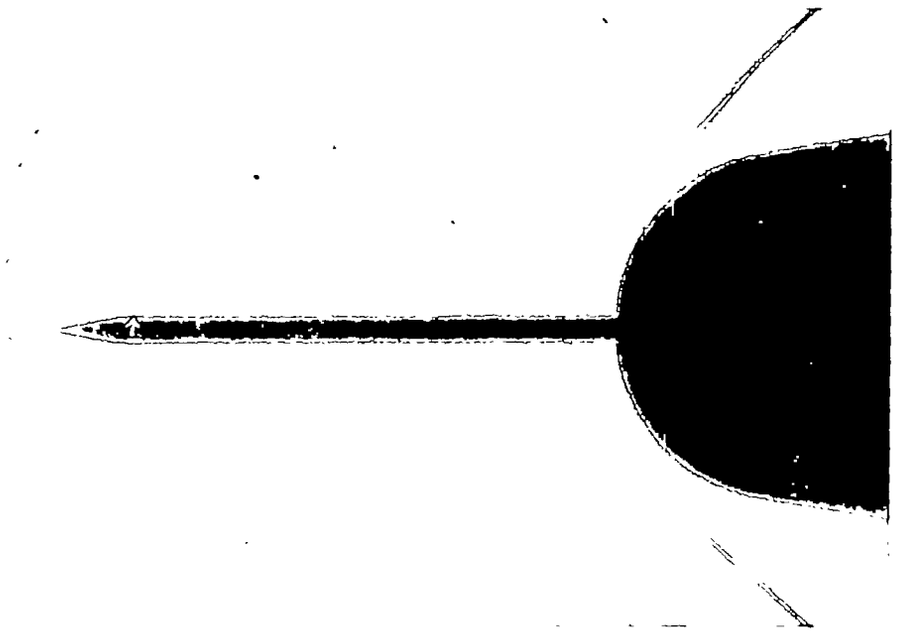

$\frac{l}{r_n} = 3.5$

L-75102

Figure 6.- Concluded.

[redacted]

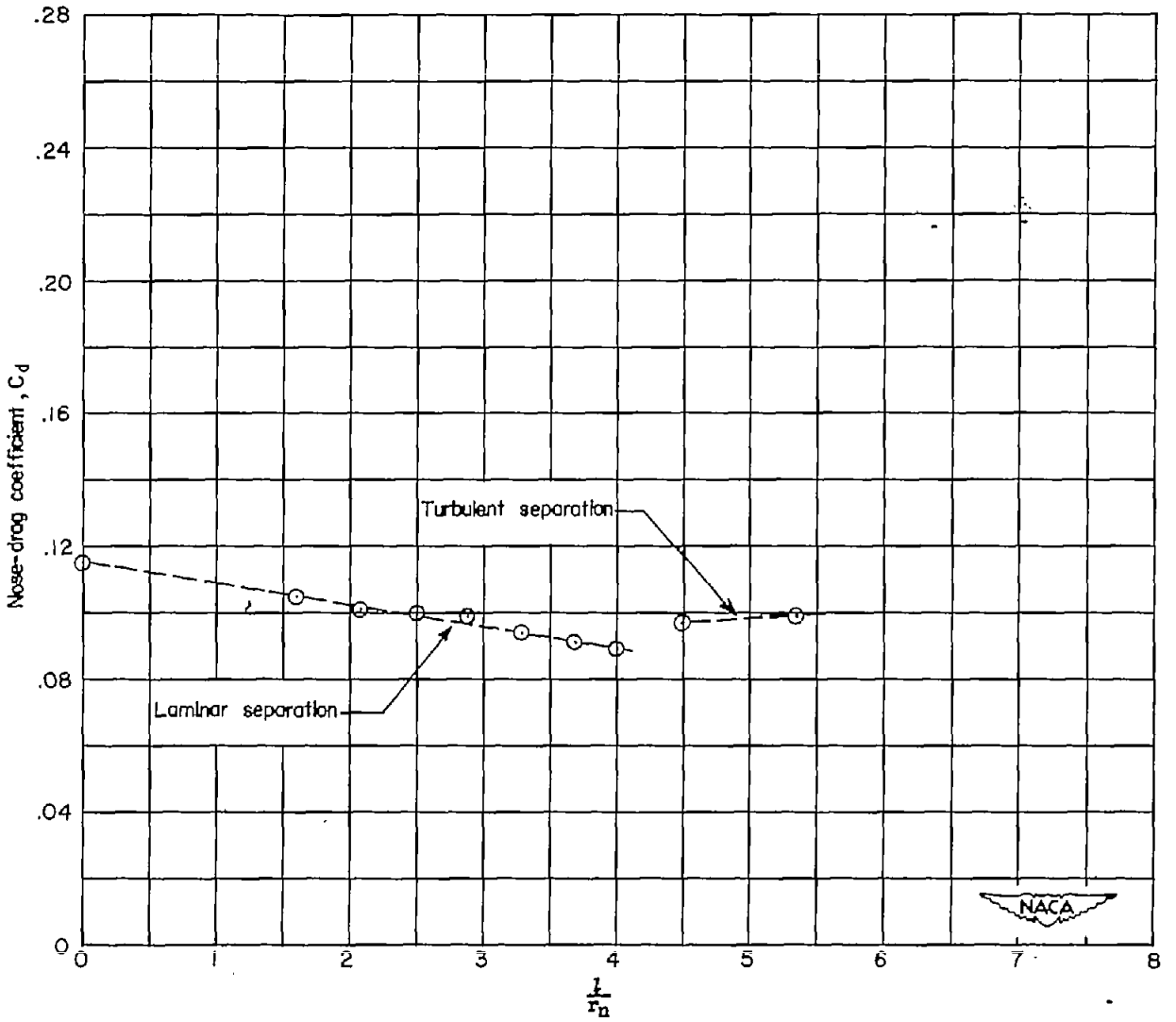

Figure 7.- Effect of rod length on drag coefficient for model 2.

[redacted]

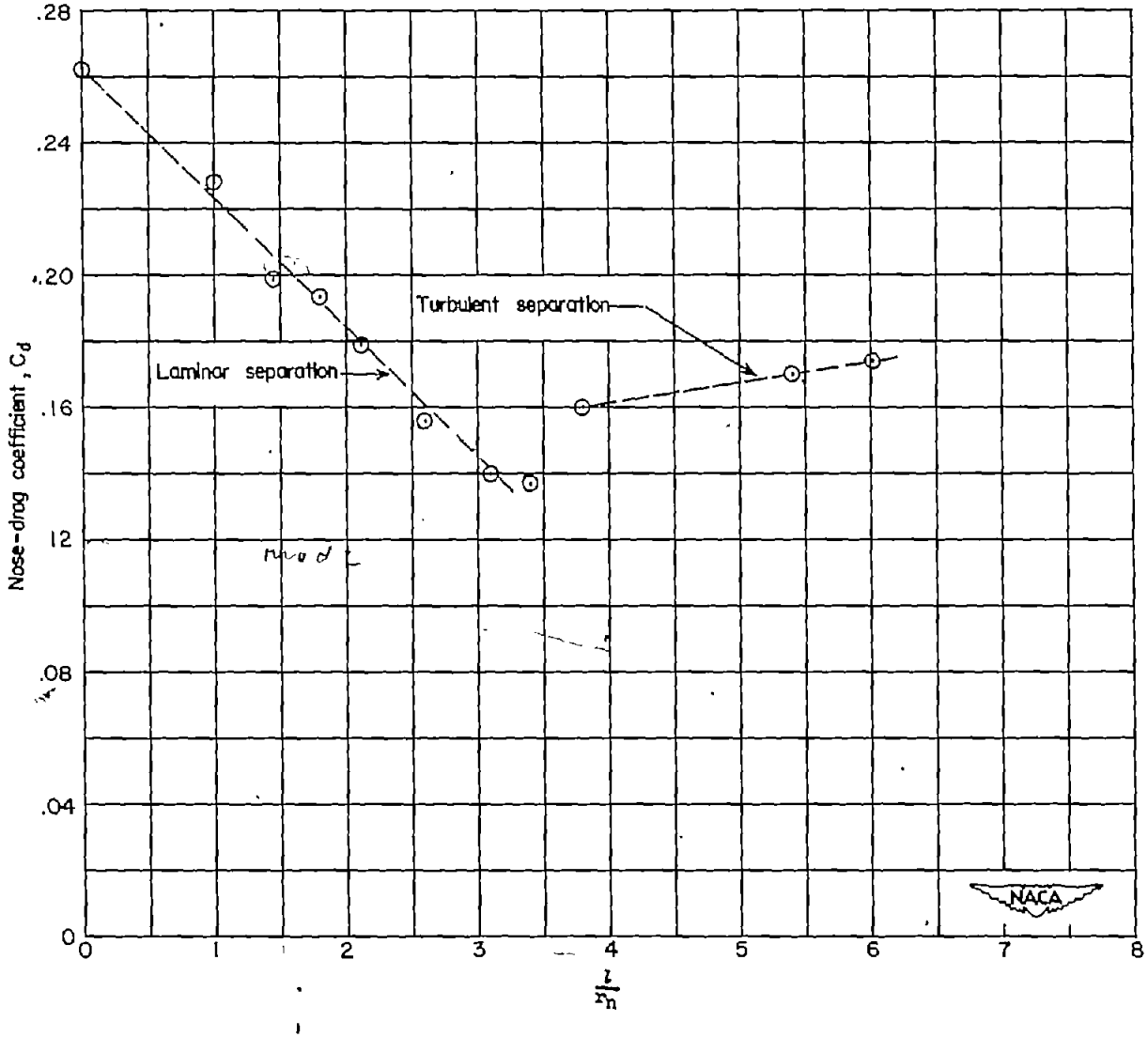

Figure 8.- Effect of rod length on drag coefficient for model 3.

NACA-Langley - 7-18-52 - 350